Distribution Agreement

In presenting this thesis as a partial fulfillment of the requirements for a degree from Emory University, I hereby grant to Emory University and its agents the non-exclusive license to archive, make accessible, and display my thesis in whole or in part in all forms of media, now or hereafter now, including display on the World Wide Web. I understand that I may select some access restrictions as part of the online submission of this thesis. I retain all ownership rights to the copyright of the thesis. I also retain the right to use in future works (such as articles or books) all or part of this thesis.

Shriya Iyer March 7, 2025

AT THE INTERFACE OF THE HUMAN HOST AND BACTERIA: STRESS SIGNALING VIA CYCLIC AMP AND CALCIUM

by

Shriya Iyer

Rabindra Tirouvanziam
Adviser

Department of Anthropology

Rabindra Tirouvanziam, PhD
Adviser

John Lindo, PhD
Committee Member

Skye Comstra, PhD
Committee Member

2025

AT THE INTERFACE OF THE HUMAN HOST AND BACTERIA: STRESS SIGNALING VIA CYCLIC AMP AND CALCIUM

by

Shriya Iyer

Rabindra Tirouvanziam, PhD
Adviser

An abstract of
a thesis submitted to the Faculty of Emory College of Arts and Sciences
of Emory University in partial fulfillment
of the requirements of the degree of
Bachelor of Science with Honors

Department of Anthropology

2025

Abstract

AT THE INTERFACE OF THE HUMAN HOST AND BACTERIA:
STRESS SIGNALING VIA CYCLIC AMP AND CALCIUM

By Shriya Iyer

Outer membrane vesicles (OMVs) play a critical role in bacterial-host interactions, influencing immune signaling and cellular responses. These OMVs influence host responses to bacterial infections, thereby regulating immunity and pathogenicity. This study investigates the differences in OMV production and host signaling activation between the laboratory-adapted strain *Pseudomonas aeruginosa* PAO1 and two clinically derived isolates. PAO1 and clinical isolates were cultured under controlled conditions, and OMVs were isolated using size-exclusion chromatography. Nanoparticle tracking analysis (NTA) quantified OMV production, while a bioluminescence assay measured cAMP and calcium signaling activation in a THP-1 monocyte cell line through CREB and NFAT reporter systems.

PAO1 exhibited a higher OMV yield per cell but showed a decreasing trend in production over time, whereas clinical isolates maintained relatively stable OMV output. Bioluminescence assays demonstrated that PAO1 OMVs elicited a consistent, dose-dependent activation of CREB and NFAT, aligning with expected cAMP and calcium stimulation. In contrast, the clinical isolates displayed more variable activation patterns, with fluctuations in NFAT and CREB responses.

These findings highlight strain-specific differences in OMV biogenesis and signaling capacity. The observed variation in cellular activation suggests that clinical isolates may have evolved distinct OMV-mediated strategies to modulate host responses. Further investigations into these mechanisms will provide insight into the evolutionary pressures shaping human immune responses to bacterial pathogens.

AT THE INTERFACE OF THE HUMAN HOST AND BACTERIA: STRESS SIGNALING VIA CYCLIC AMP AND CALCIUM

By

Shriya Iyer

Rabindra Tirouvanziam, PhD
Adviser

A thesis submitted to the Faculty of Emory College of Arts and Sciences
of Emory University in partial fulfillment
of the requirements of the degree of
Bachelor of Science with Honors

Department of Anthropology

2025

Acknowledgements

I would like to express my deepest gratitude to my research mentor, Dr. Deepali Luthra, and my PI, Dr. Rabindra Tirouvanziam, for their invaluable mentorship and feedback. Their guidance has been instrumental in shaping me as a researcher, challenging me to think more critically and refine my approach. I sincerely appreciate their time, patience, and unwavering support throughout this journey.

I am also incredibly grateful to my thesis committee members, Dr. John Lindo and Dr. Skye Comstra, for their generous commitment of time and expertise.

I would also like to extend my gratitude to the entire Tirouvanziam Lab for their support throughout this process. A special thank you to Maria Parilla for her guidance in teaching me many of the protocols used in this thesis and for her encouragement along the way.

Finally, I am deeply thankful for my family and friends, whose unwavering support has kept me motivated—especially during 12-hour experiment days and late nights in the lab.

Table of Contents

List of Tables and Figures

1. Introduction

Living organisms continuously receive and respond to signals from their environment. The cells that form these living systems detect and integrate information from both external surroundings and internal conditions. Signal transduction is the process by which cells transmit information from sensory molecules, such as cell surface receptors, through signaling molecules to various intracellular components that trigger specific responses. This coordination of signaling molecules regulates the functions of the many cells that comprise both simple and complex organisms, including humans. The intricate networks of signal transduction pathways allow cells to manage essential processes such as metabolism, movement, growth, division, differentiation, and death. As a result, signaling is a fundamental aspect of all cellular life.

1.1 Host and environment

1.1.1 Signal transduction

Signal transduction, a fundamental aspect of cell regulation, involves various pathways for binding of signaling molecules, known as ligands, to receptors that trigger events inside the cell. Ligand binding alters the receptor's protein conformation, thereby activating nearby effector proteins to catalyze the production, release, or influx of small molecules, also called secondary messengers (Newton et al., 2016). These messengers rapidly diffuse to other cellular proteins to modify their activities in response to the receptor's signal.

1.1.2 Role of secondary messengers in biological systems

Secondary messengers are integral to the cell's ability to sense and respond to environmental changes. By generating spikes in these messengers, cells can amplify signals and coordinate precise responses to stimuli (González-Espinosa and Guzmán-Mejía, 2014). These molecules are present at low concentrations in the cytosol of resting cells, but they are rapidly produced, imported from the extracellular milieu, or released from intracellular stores upon stimulation, such as intracellular stimuli or ligand binding to extracellular receptors (González-Espinosa and Guzmán-Mejía, 2014). Dysregulation of secondary messenger pathways is often associated with disease (Newton et al., 2016).

Among the various classes of secondary messengers—including cyclic nucleotides, lipid derivatives, small bioactive molecules, and ions—cyclic adenosine monophosphate (cAMP) and calcium ions (Ca^{2+}) are the most extensively studied (González-Espinosa and Guzmán-Mejía, 2014). cAMP and Ca^{2+}ions influence nearly every aspect of cellular life across a wide range of organisms, from protozoans and plants to humans (Hofer and Lefkimmiatis, 2007). The interconnectedness of these two molecules is exemplified by the fact that the cAMP pathway is modulated by Ca^{2+} levels (Hofer, 2012). Notably, mammalian adenylyl cyclases, which synthesize cAMP, are regulated by Ca^{2+} signaling—either directly via Ca^{2+} ions or indirectly through enzymes like CaM kinase, protein kinase C (PKC), or calcineurin (Halls and Cooper, 2011).

1.1.2.1 Cyclic adenosine monophosphate (cAMP)

Cyclic AMP (cAMP), a hydrophilic small molecule and the first identified secondary messenger, plays a pivotal role in cellular processes, including memory, metabolism, gene regulation, and immune function in both health and disease states (Sassone-Corsi, 2012) (Serezani et al., 2008). The synthesis of cAMP is catalyzed by adenylyl cyclase (AC) following receptor activation, leading to the conversion of adenosine monophosphate (AMP) into cAMP. Once produced, cAMP activates protein kinase A (PKA), which phosphorylates serine and threonine residues on downstream effector proteins, thereby modulating various cellular responses (Newton et al., 2016). A key target of PKA is the cAMP response element-binding protein (CREB), a transcription factor that regulates genes involved in cell cycle, and metabolism (Patra et al., 2024).

1.1.2.2 Calcium ions

Calcium ions (Ca^{2+}) serve as ubiquitous intracellular messengers, playing an essential role in processes such as muscle contraction, synaptic transmission, gene expression, and immune signaling. Cells maintain a tightly regulated intracellular Ca^{2+}concentration, with a steep gradient between the cytoplasm and extracellular environment, estimated at approximately 20,000-fold (Clapham, 2007). Cells are naturally at low cytoplasmic Ca^{2+}concentrations, but Ca^{2+} ions are easily mobilized upon stimulation, triggering specific cellular responses. Unlike other secondary messengers that must be synthesized enzymatically upon stimulation, Ca^{2+} ions are immediately available in large quantities. This rapid mobilization is achieved by influx of Ca^{2+} through membrane-embedded channels separating the cytoplasm from calcium stores, thereby releasing Ca^{2+} across the existing electrochemical gradient (Endo, 2006).

1.1.3 cAMP and Ca^{2+} regulation of membrane channels

1.1.3.1 CFTR channel

cAMP and Ca^{2+}spikes regulate numerous channels within the body that play key roles at the host-environment interface. One such channel, the cystic fibrosis transmembrane conductance regulator (CFTR), is an anion channel essential for maintaining salt and fluid balance across epithelial membranes (Levring et al., 2023). Proper CFTR function is essential for controlling mucus hydration and viscosity, which are key to airway clearance (Hanssens et al., 2021). CFTR activity is primarily regulated by cAMP. Elevated intracellular cAMP levels activate PKA, which phosphorylates CFTR, increasing its open probability and facilitating anion transport into the airway lumen (Murabito et al., 2023). This may control the osmolarity or the pH of the extracellular milieu if chloride or bicarbonate ions, respectively, pass through CFTR, ensuring optimal mucus biophysical properties. Ca^{2+} signaling further supports airway fluid homeostasis by promoting activation of calcium-activated channels, which also can impact fluid secretion (Bozoky et al., 2017). Together, cAMP and Ca^{2+} spikes regulate CFTR and other channels, which can, in turn, influence pathogen-host interactions at mucosal surfaces (e.g., lung and gut). Through these channels, cAMP and Ca^{2+} ions contribute towards both the establishment of a stable commensal microbiome in the gut and the elimination of pathogenic bacteria via mucus clearance in the lung.

In CF, mutations in the CFTR gene disrupt the function of this critical channel (Chen et al., 2021). Disease-causing mutations lead to the absence of CFTR proteins (stop mutations), or to defective CFTR proteins that are misprocessed by the endoplasmic reticulum and/or fail to reach the cell membrane and/or show defective anion transport (missense mutations). The F508del mutation, the most commonly detected among CF patients, involves a specific amino acid deletion within the CFTR protein sequence (Chen et al., 2021). The defective CFTR channel and resulting imbalances in ion and fluid transport create an environment conducive to infection. *Pseudomonas aeruginosa*, an opportunistic pathogen, frequently colonizes the CF lung, accelerating the decline in pulmonary function. This pathogen exhibits substantial resistance to both innate immune defenses and antibiotics, enabling it to evade host responses (Malhotra et al., 2019). Calcium has been shown to accumulate in the pulmonary fluids of CF patients, and in response to these elevated calcium levels, *P. aeruginosa* increases the production of secreted virulence factors through a calcium-binding protein, known as PA4107 (Sarkisova et al., 2014). These adaptations further enhance the pathogen's ability to persist in the CF lung, accelerating disease progression.

1.1.3.2 TRP channel

Transient receptor potential (TRP) channels are essential signaling proteins that function as sensors for a variety of cellular and environmental cues. Mammals express 28 distinct TRP channel proteins, which are classified into seven subfamilies based on amino acid sequence homology. These channels are crucial for sensory responses to stimuli such as heat, cold, pain, stress, vision, and taste (Zhang et al., 2023). TRP channels are not only involved in these sensory functions but also play a significant role in cellular signaling by being targets of phosphorylation by PKA, the primary effector of cAMP signaling (Cantero et al., 2015). This links TRP channels to the broader signaling pathway involving cAMP.

TRP channel activation leads to a rise in intracellular calcium, either through the channels themselves or via other signaling mechanisms, such as G-protein coupled receptors (Hasan and Zhang, 2018). This Ca^{2+} ion influx is particularly relevant in the context of CF, where TRP channels like TRPA1, TRPC6, TRPV4, and TRPV6 are activated by pathogens such as *P. aeruginosa* (Grebert et al., 2019). The resulting increase in intracellular Ca^{2+} levels triggers the production of inflammatory mediators, amplifying the inflammatory response. In this way, TRP channels serve as crucial integrators of both cAMP and Ca^{2+} signaling, linking cellular responses to environmental stimuli and contributing to disease processes like those observed in CF.

1.2 Host-pathogen interactions

Pathogens can interfere with signal transduction in host cells as a survival tactic. Many successful bacterial pathogens evade immune detection by modifying their surface, disrupting signaling pathways triggered by receptor-ligand interactions, or utilizing alternative receptors (Rosenberger and Finlay, 2003). Some pathogens exploit the damaging effects of an excessive inflammatory response on the host, while others survive by suppressing or evading the host immune response. By altering host signaling, these pathogens impair the intercellular communication required to clear the infection.

1.2.1 Pathogen-associated molecular patterns and damage-associated molecular patterns

Host cells recognize the presence of a pathogen through pathogen-associated molecular patterns (PAMPs) present on the surface of pathogenic microorganisms, for example, flagellin and pili (De Lorenzo et al., 2018). They are recognized by pattern recognition receptors (PRRs)

expressed on both immune and nonimmune cells, activating proinflammatory and antimicrobial responses in innate immune cells. In contrast, cells release DAMPs as endogenous danger signals that alert the innate immune system to cell damage, microbial invasion, and in general, response to stressors (Tang et al., 2012).

Lipopolysaccharide (LPS), a key structural component of the outer membrane of most gram-negative bacteria, is a prototypical PAMP that can be recognized by multiple host receptors, including Toll-like receptors (TLRs). Recognition of PAMPs may also activate intracellular scaffolds named inflammasomes, leading to the release of proinflammatory cytokines (Qin et al., 2022). However, pathogens like *Pseudomonas aeruginosa* can evade or promote tolerance by the host immune system by decreasing the secretion and extracellular presence of virulence factors or by delivering them directly into host cells. A critical component of this immune evasion strategy is outer membrane vesicles (OMVs), which transport bacterial proteins, lipids, and nucleic acids to host cells, bypassing immune defenses and promoting bacterial colonization (Qin et al., 2022).

1.2.2 Extracellular vesicles and outer membrane vesicles

Eukaryotic cells release extracellular vesicles (EVs) as part of a wide range of biological processes, from regulating metabolism in normal physiology to playing a role in pathological conditions such as infection and cancer. EVs, by definition, are nanosized lipid particles secreted by nearly all living cells, carrying bioactive molecules that move between cells and transmit signals to regulate processes like cell growth. (Zou et al., 2022). In host cells, EVs can help combat bacterial infections by removing damaged membranes, expelling and neutralizing bacteria, viruses, and toxins, and activating both innate and adaptive immune responses throughout the body.

In Gram-negative bacteria, extracellular vesicles are referred to as outer membrane vesicles (OMVs). These spherical, non-living nanostructures, ranging from 20 to 300 nm in size, originate from the bacterial cell envelope (Sartorio et al., 2021). Their membranes contain lipopolysaccharides, glycerophospholipids, and outer membrane proteins, while their interior compartments house proteins, DNA, and RNA molecules (Xie et al., 2024). OMVs can travel long distances from their parent bacteria, delivering toxins and immunomodulatory molecules to remote sites without direct bacterial contact. One mechanism by which OMVs facilitate immune evasion is by acting as decoys for antimicrobial agents such as antibodies, weakening host immune defenses (Tiku and Tan, 2021). For example, OMVs from *Pseudomonas aeruginosa* carry

virulence factors such as alkaline phosphatase, phospholipase Cs, β-lactamase, and the CFTR Inhibitory Factor (Cif), which impair bacterial clearance in the lungs of CF patients and aid in outcompeting other microbial species in the lung (Augustyniak et al., 2022) (Xie et al., 2024).

OMVs are essential in shaping host-bacteria interactions, particularly through the delivery of various virulence factors, including toxins, siderophores, immune evasion proteins, adhesins, and antibiotic resistance factors (Sangiorgio et al., 2024). OMVs also play a key role in immune modulation by carrying immunogenic molecules such as LPS, flagellin, and peptidoglycan, which stimulate host immune responses via TLRs. Encapsulation within vesicles ensures the concentrated and protected delivery of these factors to host cells, increasing their potency while shielding them from immune detection and extracellular degradation by host proteases (Sangiorgio et al., 2024). The process of OMV entry into eukaryotic host cells can occur via mechanisms like endocytosis, phagocytosis, and membrane fusion, depending on the vesicle type and the target cell. Overall, OMVs serve as extensions of the bacteria, allowing them to exert influence on host cellular processes, including signal transduction pathways such as cAMP and Ca^{2+} regulation.

1.2.3 The effect of pathogens on cAMP and Ca^{2+} levels

Pathogenic bacteria commonly increase cAMP levels in neighboring host cells through various mechanisms, including the direct release of cAMP, the induced production of cAMP via secreted bacterial adenylyl cyclase (AC) toxins, or the stimulation of host ACs (McDonough and Rodriguez, 2012). Some bacterial pathogens are also able to alter the host's intracellular Ca^{2+} levels by activating Ca^{2+} flux across the plasma membrane and, releasing Ca^{2+} from intracellular stores into the cytosol (King et al., 2020). In some cases, alterations in host intracellular Ca^{2+} levels have been implicated in promoting bacterial adherence and entry into host cells (King et al., 2020).

1.2.4 Altered cAMP and Ca^{2+} levels impair immune function

High intracellular cAMP levels can hinder innate immune functions by altering the expression of inflammatory mediators like IL-10, diminishing the phagocytic response, and decreasing the intracellular elimination of ingested pathogens (McDonough and Rodriguez, 2012; Ernst et al., 2019). Additionally, in epithelial cells, high intracellular cAMP levels activate the CFTR channel, leading to chloride efflux and flushing of the luminal content, an evolutionary strategy used by certain bacteria for clearing out the preexisting microbiota (Nguyen et al., 2021). High cAMP also

blocks the TRP channel of melastatin type 8 (TRPM8) channel, which initially induces mucus secretion and leukocyte recruitment in cold ambient temperatures (De Petrocellis et al., 2007; Nguyen et al., 2021). Interestingly, TRPM8 activation leads to a Ca^{2+} spike that leads to delayed CFTR activation (and eventual mucus flushing). A sustained increase in intracellular Ca^{2+} levels is a hallmark of cell injury. Elevated calcium levels can disrupt the cytoskeleton, contribute to cell swelling, and alter permeability of the plasma membrane, mitochondrial membrane, or endoplasmic reticulum membrane, leading to cellular damage (Rajasekaran et al., 2011).

1.3 Significance of research project

1.3.1 Pathogenic bacteria (*Pseudomonas*)

This project examines one main bacterial pathogen: *Pseudomonas aeruginosa*. *Pseudomonas aeruginosa* is an environmental bacterium that causes opportunistic infections in humans. It is ubiquitous, found in water sources, on the surfaces of fruits and vegetables, in sinks, showerheads, and on medical devices such as catheters (Saussereau and Debarbieux, 2012). *P. aeruginosa's* adaptability to diverse growth conditions is enabled by a wide array of metabolic pathways and regulatory genes. The bacterium's nutritional flexibility, numerous virulence factors, and high antibiotic resistance make it particularly challenging to eradicate, especially in chronic lung infections in CF patients (Wu et al., 2015). For research purposes, the PAO1 laboratory strain serves as the standard reference strain for studying *P. aeruginosa* genetics, as well as the physiological and metabolic functions of this bacterium (Klockgether et al., 2010).

P. aeruginosa depends on cAMP signaling for critical functions, including virulence factor production and biofilm formation (Fuchs et al., 2010). Calcium signaling also plays a critical role in *P. aeruginosa* virulence and adaptive responses. The bacterium detects external Ca^{2+} levels as a physiological cue, triggering changes in the abundance of intracellular proteins and the secretion of virulence factors such as alginate, pyocyanin, and proteases (Guragain et al., 2016). These Ca^{2+}-induced shifts enhance biofilm formation and increase bacterial motility, facilitating persistence in host tissues. Additionally, Ca^{2+} levels can regulate the expression of proteins involved in iron acquisition, nitrogen metabolism, and stress responses (Guragain et al., 2016). These findings underscore the critical regulatory role of secondary messengers in *P. aeruginosa* virulence.

1.3.2 CREB- and NFAT-responsive human monocyte reporter cell lines

Monocytes play a crucial role in the mammalian immune system, serving as key defenders against bacterial infections. Their ability to sense and respond to bacterial components is essential for orchestrating innate immune responses. To investigate the signaling pathways activated in monocytes upon bacterial exposure, we employ the THP-1 cell line—a spontaneously immortalized monocyte-like line derived from a child with acute monocytic leukemia—as a model for primary human monocytes (Bosshart and Heinzelmann, 2016). This study specifically utilizes THP-1 CRE-Luc2 and THP-1 NFAT-Luc2 cell lines, which express a luminescent luciferase reporter gene regulated by intracellular cAMP and Ca^{2+} levels, respectively.

As mentioned previously, the cAMP signaling pathway is initiated through adenylyl cyclase activation, which increases intracellular cAMP levels. This, in turn, activates protein kinase A (PKA), leading to the phosphorylation of cAMP response element-binding protein (CREB), a transcription factor that binds to CRE within target gene promoters, enhancing their transcription (Wang et al., 2018). In the THP-1 CRE-Luc2 line, this cascade drives the expression of the luciferase reporter gene, providing a quantifiable readout of cAMP signaling activity **(Figure 1A)**. Calcium signaling involves the activation of calcineurin by Ca^{2+}-bound calmodulin. Calcineurin dephosphorylates the nuclear factor of activated T cells (NFAT), enabling its translocation into the nucleus, where it regulates gene transcription (Zhang et al., 2024). The THP-1 NFAT-Luc2 line **(Figure 1B)** allows us to assess Ca^{2+}-mediated signaling activation in response to bacterial stimuli.

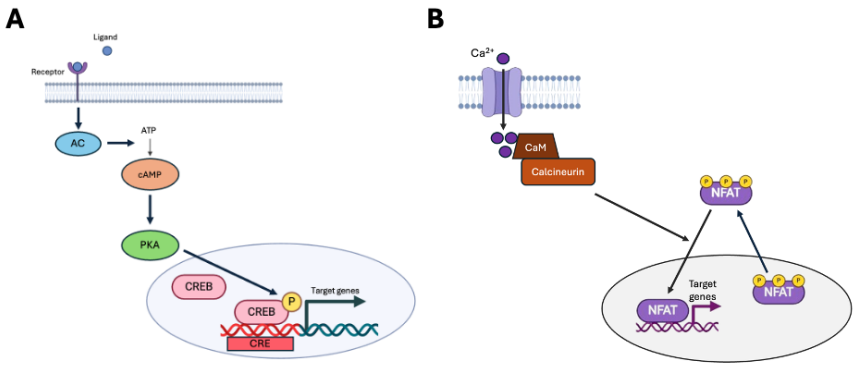

Figure 1. Principle of cAMP- and Ca^{2+}- reporter cell lines.
Human monocyte lines used report on changes in intracellular cAMP and Ca^{2+} levels caused by exposure to P. aeruginosa OMVs via CREB- [**(A)**, inspired by Wang et al., 2018] and NFAT- [**(B)**, inspired by Zhang et al., 2024] driven luciferase expression.

1.3.3 Project: investigating the effects of *P. aeruginosa* OMVs on immune cell signaling.

This study examines OMVs as central agents in host-microbe and interactions. As previously mentioned, gram-negative bacteria release OMVs that serve as versatile secretion and transport mechanisms. Given their ability to influence host cellular pathways, including signal transduction mechanisms such as cAMP and calcium regulation, OMVs are not only

fundamental to bacterial survival and infection but also critical to understanding host-pathogen interactions. We anticipate that exposure to OMVs from bacterial supernatants will lead to measurable changes in cAMP and calcium levels in target host cells. Specifically, given the role of *P. aeruginosa* in modulating these pathways in epithelial cells, **our central hypothesis is that *P. aeruginosa* OMVs alters cAMP and Ca^{2+} signaling in human monocytes**, key players in infection clearance and regulation of inflammation. To test this hypothesis, we leverage the luminescent reporter cell lines described above. This is particularly relevant in the context of CF, where chronic *P. aeruginosa* infections are associated with decade-long inflammation and progressive lung damage.

2. Methods

2.1 Bacterial culture

An overnight primary culture of *P. aeruginosa* strains was started by inoculating 5 ml of Luria-Bertani (LB) broth in a 14 ml snap cap culture tube in aseptic conditions. For PAO1 and clinical isolate 2 (CF2), cultures were initiated from previously streaked agar plates, while glycerol stock was used for Clinical Isolate 1 (CF1). The tube was incubated overnight in a 37°C shaker at 220 rpm. The incubation duration varied by strain, with PAO1 and CF1 incubated for approximately 14 hours, while CF2 was optimized to grow for closer to 24 hours before subculturing due to slower initial growth. For the secondary culture, 5% of primary overnight culture was transferred to LB (100 mL for PAO1, 140 mL for both clinical isolates) in a sterile 250 mL Erlenmeyer flask under an aseptic zone. The mixture was homogenized by pipetting up and down and incubated at a 37°C shaker at 220 rpm for bacterial growth.

At the zero-hour timepoint and each two-hour timepoint afterwards, 15 mL of culture were collected for analysis. The sample was centrifuged at 3,000 × g for 10 minutes to separate intact bacterial cells from the supernatant and carefully transferred to a new sterile 50 mL conical tube, ensuring no disruption of the pellet. For quality control, spot plating was performed on 1.5% LB agar plates at each timepoint to determine colony-forming units (CFU/mL). Additionally, optical density (OD_{600}) measurements using a spectrophotometer (Molecular Devices, SpectraMax M2e) were recorded to track bacterial growth. This procedure was followed for all bacterial strains.

2.2 OMV isolation

The overall procedure is depicted in **Figure 2**. In brief, Izon 70 nm qEV size-exclusion columns were used for OMV isolation following an initial concentration step, precisely, 15 mL of bacterial supernatant was first concentrated using an Amicon Ultra Centrifugal Filter (50 kDa) to obtain a volume 500 µL before loading onto the column. The upper and lower caps of the column were then removed, allowing residual PBS to drain. The column was washed by adding 20 mL of PBS, which was allowed to flow through completely.

For OMV isolation, 500 µL of the concentrated bacterial sample was carefully loaded onto the washed column, allowing the sample to flow into the resin by removing the bottom cap. Once fully absorbed, 500 µL of PBS was added five times, totaling 3.0 mL of flowthrough (500

µL sample and 2.5 mL PBS), and these fractions were discarded. Next, 500 µL of PBS was added three more times, and this 1.5 mL of collected fractions were transferred into a 1.5 mL Eppendorf tube and stored on ice for further processing. Before running a new sample, the qEV column was cleaned with 20 mL of PBS to remove residual material.

For final OMV concentration, the 1.5 mL of collected sample was loaded into an Amicon Ultra Centrifugal Filter (10 kDa), with the cap facing up. The column was spun at 3,000 × g for 10 minutes, followed by additional 1–2 minute spin cycles until the volume was reduced to 500 µL. The column was then flipped cap-side down and spun again at 3,000 × g for 1 minute to collect the entire 500 µL sample into the cap. The final concentrated sample was transferred to a 1.5 mL Eppendorf tube and placed at -80°C for future use. The 10 kDa Amicon filter was washed between uses but was not used more than three times before replacement.

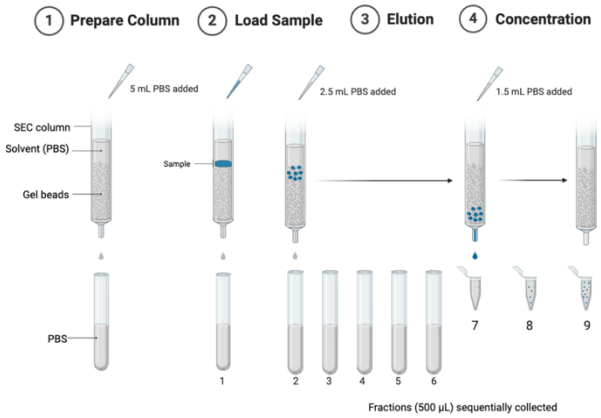

Figure 2. OMV isolation procedure
(courtesy of Ziya Jiwani)

2.3 Nanoparticle tracking analysis (NTA)

To quantify OMV counts, the NanoSight 300 (Malvern Panalytical), equipped with the NanoSight 96-well sampling assistant and NTA software, was used for data acquisition and analysis. Prior to sample loading, the 96-well plate was thoroughly washed with deionized (DI) water to eliminate potential contaminants. OMV samples were then diluted in sterile 1x phosphate-buffered saline (PBS), with a sample known to contain EVs selected as a reference. Experimental wells were assigned specific sample names, and corresponding dilution factors were inputted into the system, with a 20x dilution determined to be optimal for maintaining countable OMV concentrations. Periodic checks were conducted throughout the experiment to ensure system integrity and address any deviations to maintain data accuracy.

2.4 THP-1 cell culture, OMV exposure and luminescence assay

THP-1 cells (THP-1 CRE-Luc2 - TIB-202-CRE-LUC2; THP-1 NFAT-Luc2 - TIB-202-NFAT-LUC2) were purchased from ATCC and propagated per manufacturer's guidelines. For

OMV exposure and luminescence quantification, THP-1 cells were seeded at 50,000 cells per well, with the exception of wells designated for luciferase and media + substrate controls. To minimize signal interference and ensure accurate luminescence measurements, a 96-well white flat-bottom plate was used with empty wells between sample arranged in a zig-zag pattern.

Positive controls were, for the CREB reporter line (cAMP signaling), forskolin at 2.5, 5, 10, and 20 μM concentrations, and for the NFAT reporter line (Ca^{2+} signaling), ionomycin at 0.25, 0.5, 1, and 2 μM concentrations. PAO1 OMVs were tested at a concentration of 8, 40, and 200 million OMVs per condition, while assays using pooled OMVs from each bacterial strain were tested at 50, 100, and 200 million OMVs per condition. Bright-Glo Reagent (Promega Corporation, Madison, WI) was used to generate the luminescent signal across all conditions, with luciferase serving as a positive control for the substrate. Luminescence measurements were recorded at 4- and 8-hour timepoints to evaluate cellular activation in response to each condition.

3. Results

3.1 Growth rate of the PAO1 lab-adapted strain of *P. aeruginosa*

To study the growth rate of *P. aeruginosa* PAO1, OD_{600} measurements were recorded at two-hour intervals over an eight-hour period across five independent collections **(Figure 3)**. As expected, the growth curves demonstrated a steady increase in bacterial cell density over time. After multiple technical repeats, it was determined that timepoint six (T6) represented the exponential growth phase without nearing the stationary phase, indicating active bacterial proliferation. As a result, T6 was selected for all downstream applications, including quality control, OMV count, and luminescence assays. Additional collections were subsequently performed with measurements taken exclusively at T6.

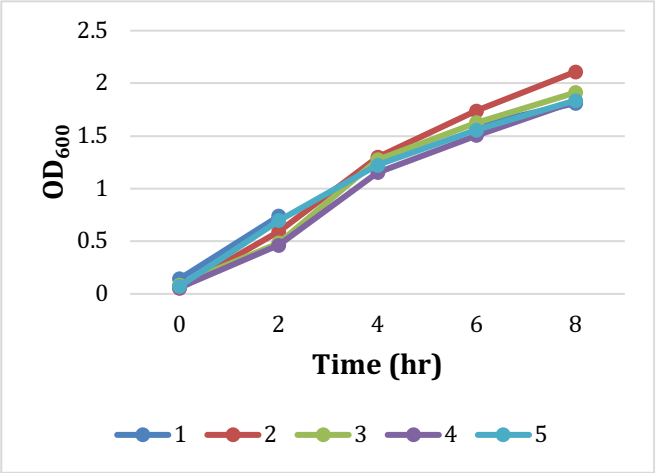

Figure 3. Growth curves of PAO1.
OD_{600} measurements were recorded at 2-hour time intervals across five independent collections (Replicate 1–5). The x-axis denotes time (in hours), while the y-axis indicates OD_{600}, which serves as a proxy for bacterial cell density. The graph shows growth dynamics at each collection.

To confirm OD readings, spot plating of PAO1 was performed at two-hour intervals to evaluate colony-forming units (CFUs) **(Figure 4)**. The plates show a progressive increase in CFUs over time, with countable colonies appearing at higher dilutions as bacterial growth progresses.

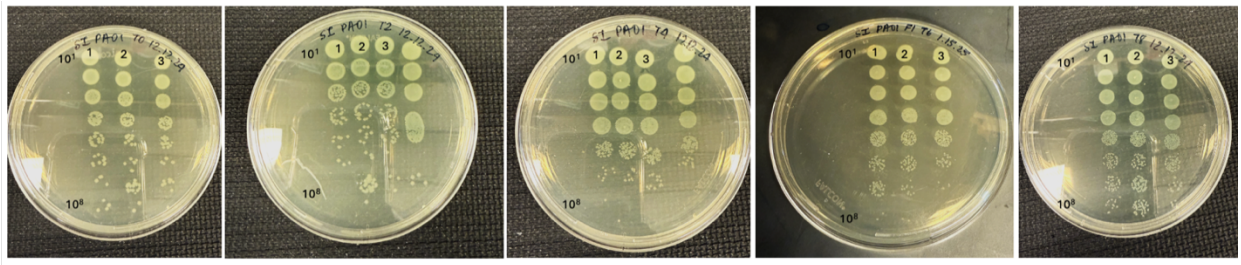

Figure 4. Spot plating of PAO1.
Representative figure displays serial dilutions from 10^1 to 10^8, with three technical repeats per dilution across timepoints T0-T8.

CFU/mL calculations at the 6-hour timepoint across 4 biological replicates confirmed consistency in bacterial density, with error bars indicating standard error **(Figure 5)**.

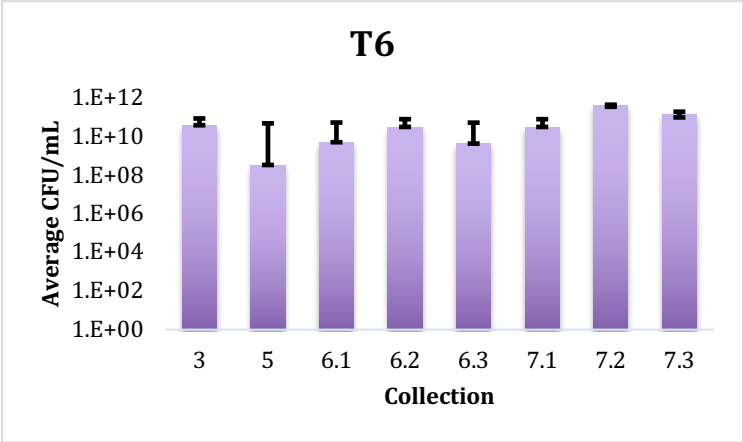

Figure 5. CFU/mL of PAO1 at the 6-hour timepoint.
For each replicate, CFU counts from three technical repeats were averaged, and values were back-calculated to represent CFU per milliliter. Error bars indicate standard error.

To ensure sample consistency across independent collections, OD_{600} measurements at T6 from collections 6.1–7.3 were compared to those from full growth curve collections (Replicates 1–5). The results showed comparable OD_{600} values, supporting consistency in bacterial growth dynamics **(Figure 6)**.

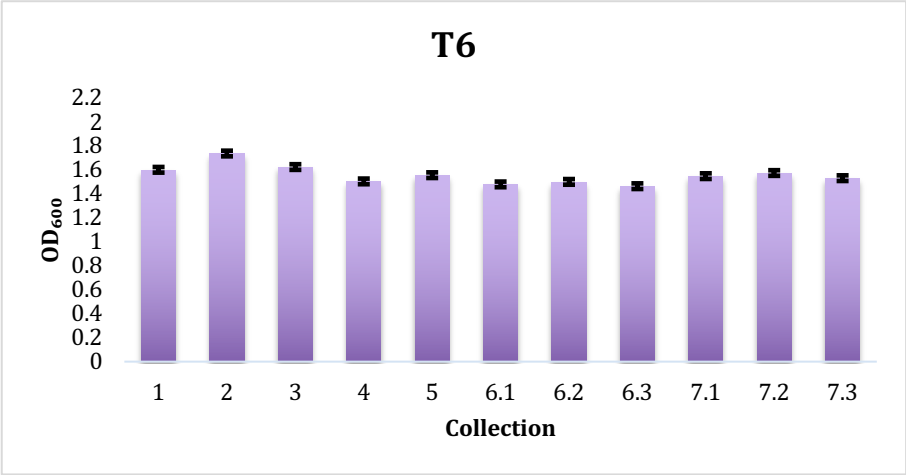

Figure 6. PAO1 OD_{600} at the 6-hour timepoint.
For collections 6.1–7.3, only samples at timepoint six were measured and collected. OD_{600} measurements for these replicates were compared with those from replicates 1–5, which underwent a full growth curve analysis. Error bars indicate standard error.

NanoSight was used to quantify OMV concentrations at multiple timepoints **(Table 1)**. Several dilutions were tested to determine the optimal dilution factor that provided OMV counts within the ideal countable range of 15–50 particles per frame. Based on these trials, a 20x dilution was found to be the most suitable for obtaining reliable OMV concentrations.

Table 1. PAO1 OMV counts from NanoSight.
This table presents NanoSight data for all isolated PAO1 OMVs, including the average particle concentration (particles/mL) and particles per frame average at various timepoints and dilution factors.

PAO1 NanoSight counts				
Replicate	**Timepoint**	**Dilution factor**	**Concentration average (particles/mL)**	**Particles / frame average**
1	T0	50x	2.18E+10	23.8
	T0	100x	1.22E+10	6.7
	T0	1000x	2.86E+10	1.6
	T0	20x	1.32E+10	36.2

	T0	10x	2.69E+09	14.7
	T2	50x	9.52E+09	10.4
	T2	100x	1.15E+10	6.3
	T2	1000x	4.29E+10	2.3
	T2	20x	5.24E+09	14.3
	T2	10x	3.07E+09	16.8
	T6	50x	1.29E+10	14
	T6	100x	9.07E+09	5
	T6	1000x	9.40E+10	5.1
	T6	20x	9.54E+09	26.1
	T6	10x	4.24E+09	23.2
	T8	50x	5.13E+09	5.6
	T8	100x	6.09E+09	3.3
	T8	1000x	1.20E+10	0.7
	T8	20x	6.68E+09	18.2
	T8	10x	5.51E+09	30.1
2	T0	100x	1.57E+11	8.6
	T2	100x	2.64E+11	14.4
	T4	100x	6.70E+11	36.6
	T6	100x	1.86E+11	10.2
	T8	100x	6.15E+11	33.6
3	T0	10x	2.99E+09	16.3
	T0	20x	4.06E+09	11.1
	T2	10x	3.52E+09	19.2
	T2	20x	3.20E+09	8.7
	T4	10x	5.14E+09	28.1
	T4	20x	1.66E+10	45.3
	T6	10x	4.00E+09	21.9
	T6	20x	5.40E+09	14.8
	T8	10x	1.12E+11	67.6
	T8	20x	8.30E+09	22.7
4	T0	10x	6.87E+09	37.5
	T0	20x	2.78E+09	7.6
	T2	10x	1.30E+09	7.1
	T2	20x	8.76E+09	23.9
	T4	10x	2.70E+09	14.7
	T4	20x	3.29E+09	9
	T6	10x	5.78E+09	31.6
	T6	20x	6.65E+09	18.2
	T8	10x	1.65E+10	90.2
	T8	20x	1.31E+10	35.8
5	T6	20x	8.97E+09	24.5
	T8	20x	1.84E+10	50.2
6.1	T6	20x	6.86E+09	18.7
6.2	T6	20x	8.46E+09	23.1
6.3	T6	20x	1.16E+10	31.7
6.4	T6	20x	4.24E+09	11.6
6.5	T6	20x	1.05E+10	28.8
6.6	T6	20x	2.23E+09	6.1

Bioluminescence assays were conducted to evaluate CREB and NFAT activation in response to PAO1 OMVs. CREB activation was measured at four and eight hours across three independent experiments (A, B, and C) **(Figure 7)**. When forskolin was used as a stimulant, relative luminescence unit (RLU) values increased up to 10 µM, after which a plateau was observed, suggesting a saturation point for CREB activation **(Figure 7A)**. When PAO1 OMVs

were tested, Experiment B showed peak activation at 40 million OMVs after 8 hours, whereas Experiments A and C exhibited either a linear increase or minimal response at both timepoints **(Figure 7B)**.

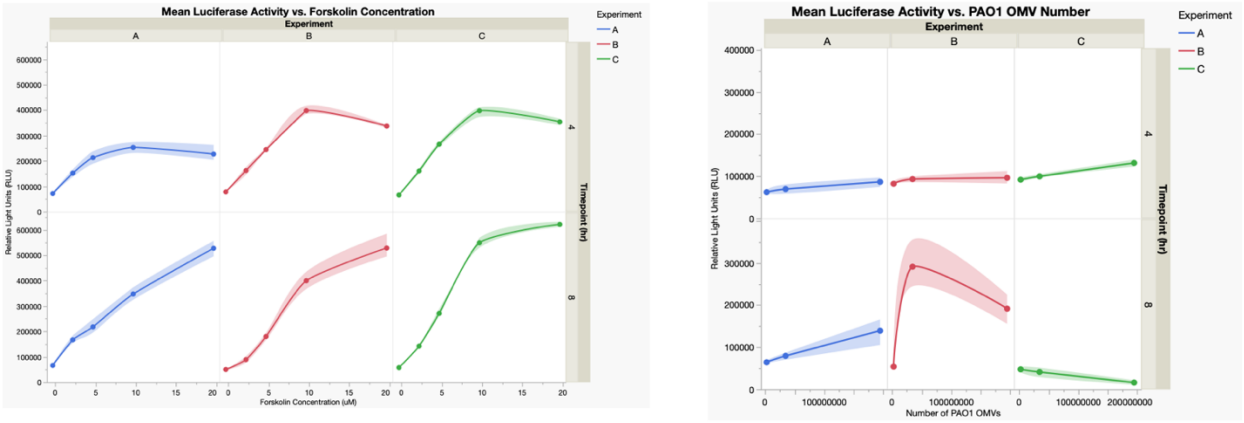

Figure 7. Activation profile of THP-1 CREB reporter line.
Luminescence was measured at 4- and 8-hour timepoints in 3 independent experiments (A, B, and C). Colored dots represent mean RLU values, with lines indicating smoothed trends. **(Left)** RLU at forskolin concentrations (0, 5, 10, 20 µM) shows an initial rise, followed by a plateau, suggesting a dose-dependent response. **(Right)** RLU at PAO1 OMV levels (8, 40, 200 x 10^6) shows peak activation in Experiment B at intermediate OMV levels, while A and C exhibit minimal responses.

Similarly, NFAT activation was assessed across five independent experiments (A, B, C, D, and E) at 4- and 8-hour timepoints **(Figure 8)**. NFAT activation increased with ionomycin stimulation up to 0.5 µM, after which no further increase was observed, indicating a threshold for NFAT response. Notably, Experiment D exhibited higher NFAT activation upon ionomycin stimulation than the other experiments, which may be attributed to a freshly prepared ionomycin stock used in that experiment, potentially increasing drug potency **(Figure 8A)**.

When PAO1 OMVs were tested, Experiments A, B, D, and E showed an increase in NFAT activation with increasing OMV concentrations, though the magnitude of activation varied. Experiment A utilized OMV concentrations of 25, 125, and 625 x10^6, which are on the higher end in terms of physiological relevance (based on our unpublished data, showing an average of 2x10^5 EVs/cell in CF sputum fluid, 1% of which are OMVs = 2x10^3 / cell). Considering that we plate 50 x10^3 THP-1 cells per well, a reasonable range for OMV exposure would thus be centered around ~100x10^6. Thus, subsequent experiments (B, C, D, and E) tested lower concentrations of 8, 40, and 200 x10^6 OMVs, resulting in a reduced activation response compared to Experiment A. This change in experimental design likely explains the more pronounced trend of NFAT activation with increasing OMV numbers in Experiment A (**Figure 8B**). Methodological differences may have also affected activation patterns across experiments.

For example, a newly prepared luciferin substrate was used in Experiments D and E, which may account for the stronger activation observed in these trials compared to Experiments B and C.

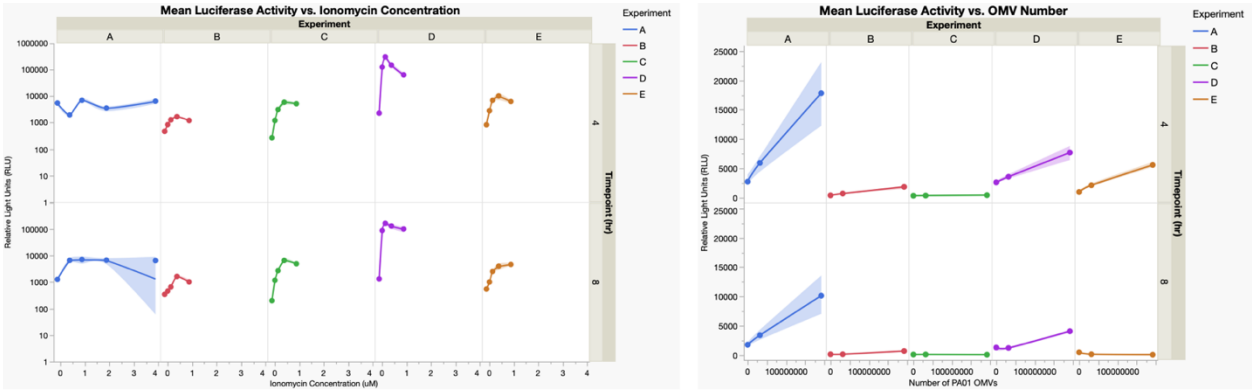

Figure 8. Activation profile of THP-1 NFAT reporter line.
Luminescence was measured at 4- and 8-hour timepoints in 3 independent experiments (A, B, and C). Colored dots represent mean RLU values, with lines indicating smoothed trends. **(Left)** RLU at ionomycin concentrations (0–4 µM) shows an initial rise, followed by a plateau, suggesting a dose-dependent response. **(Right)** RLU at PAO1 OMV levels (8, 40, 200 x 10^6) shows variability in NFAT activation, with some experiments increasing with OMV levels while others show minimal change.

3.2 CF *P. aeruginosa* clinical isolate 1 (CF1)

Similar to PAO1, OD_{600} measurements of CF1 were recorded at two-hour intervals, but attributing to a slower growth of clinical isolates in lab settings, a 12-hour time course was opted for growth curve study across six independent collections CF1 demonstrated a steady increase in bacterial density over time, with consistent trends across technical repeats **(Figure 9)**.

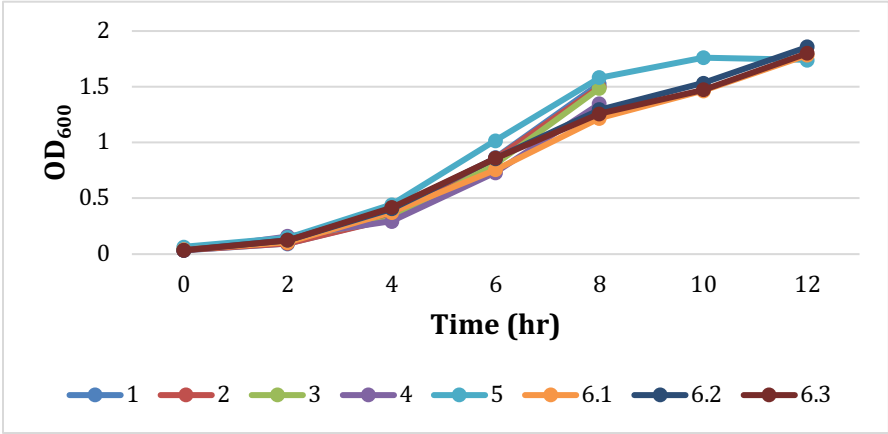

Figure 9. Growth curves of CF1.
OD_{600} measurements were recorded at 2-hour time intervals across six independent collections (Replicate 1–6). The x-axis denotes time (in hours), while the y-axis indicates OD_{600}, which serves as a proxy for bacterial cell density. The graph shows growth dynamics at each collection.

To confirm OD readings, spot plating of PAO1 was performed at two-hour intervals to evaluate CFUs **(Figure 10)**. The plates show a progressive increase in CFUs over time, with countable colonies appearing at higher dilutions as bacterial growth progresses.

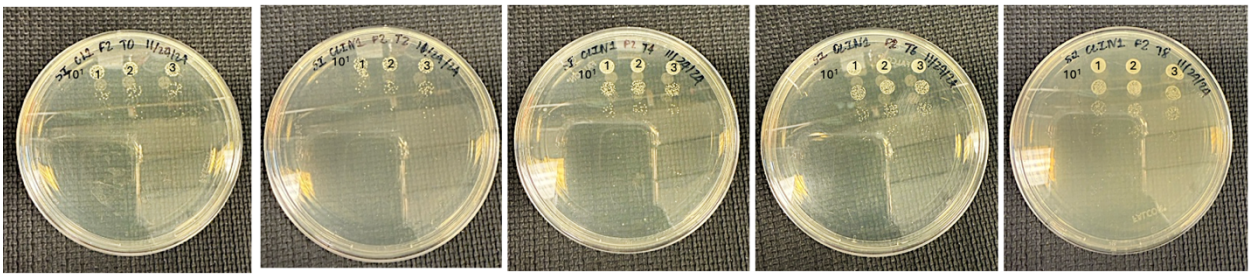

Figure 10. Spot plating of CF1.
Representative figure displays serial dilutions from 10^1 to 10^8, with three technical repeats per dilution across timepoints T0-T8.

CFU/mL calculations over time showed a general increase in bacterial density, with the highest values observed at eight hours **(Figure 11)**. Timepoints 10 and 12 are not shown due to excessively high CFU counts (too many to count, TMTC).

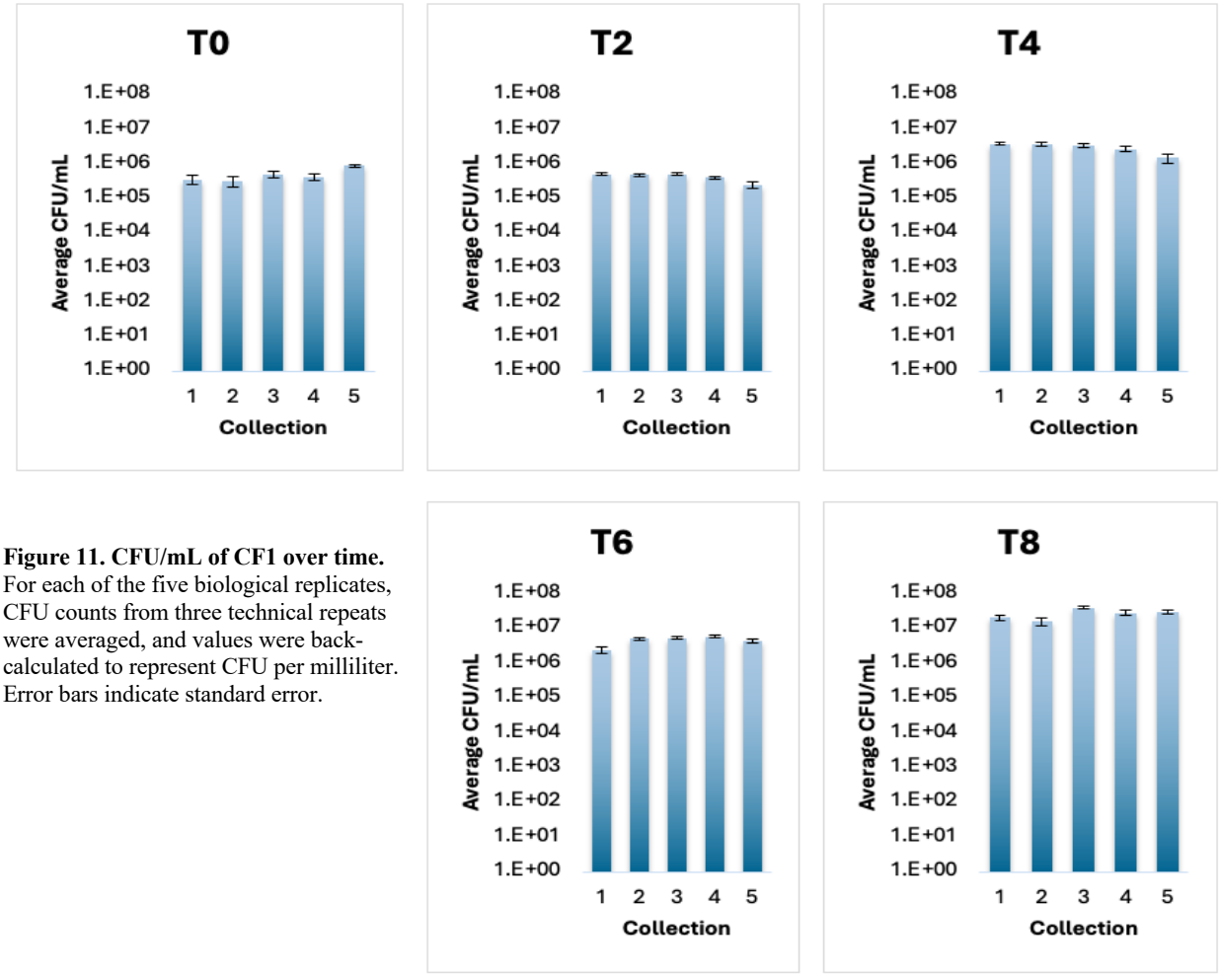

Figure 11. CFU/mL of CF1 over time.
For each of the five biological replicates, CFU counts from three technical repeats were averaged, and values were back-calculated to represent CFU per milliliter. Error bars indicate standard error.

To ensure sample consistency across independent collections, OD_{600} measurements at T6 from collections 7-9 were compared to those from full growth curve collections (Replicates 5-6.3) **(Figure 12)**. The results show comparable OD_{600}, supporting consistency in growth dynamics.

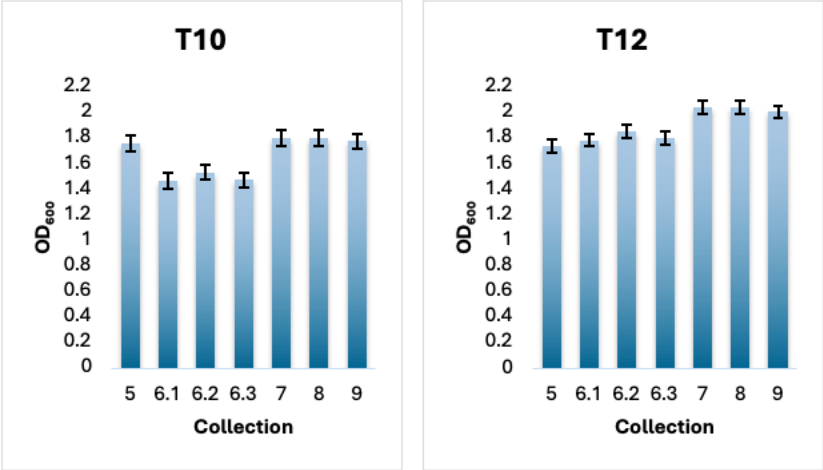

Figure 12. CF1 OD_{600} at the 6-hour timepoint.
OD_{600} measurements for these replicates were compared with those from replicates 5-6.3, which underwent a full growth curve analysis. Error bars indicate standard error.

NanoSight was used to quantify OMV concentrations from CF1 cultures at various timepoints **(Table 2)**. OMV counts showed less variability across timepoints than for PAO1 cultures **(Table 1)**, with concentrations ranging from 3.14 E+08 to 1.61 E+09 particles/mL at the two-hour timepoint and 4.66 E+09 to 6.51 E+09 particles/mL at the twelve-hour timepoint.

Table 2. CF1 OMV counts from NanoSight.
This table presents NanoSight data for all isolated CF1 OMVs, including the average particle concentration (particles/mL) and particles per frame average at various timepoints and dilution factors.

CF1 NanoSight Counts				
Replicate	**Timepoint**	**Dilution factor**	**Concentration average (particles/mL)**	**Particles / frame average**
1	T0	10x	8.20E+08	6.6
	T0	20x	7.58E+08	2.9
	T2	10x	4.35E+08	4.5
	T2	20x	3.14E+08	2
	T4	10x	4.38E+08	4.2
	T4	20x	5.28E+08	2.3
	T6	10x	1.52E+09	10.4
	T6	20x	1.34E+09	5.8
	T8	10x	1.05E+09	7.8
	T8	20x	1.03E+09	4.5
2	T0	10x	8.26E+08	4.5
	T0	20x	1.18E+09	3.2
	T2	10x	2.84E+08	1.6
	T2	20x	2.58E+08	0.7
	T4	10x	3.27E+08	1.8
	T4	20x	3.50E+08	1
	T6	10x	5.88E+08	3.2
	T6	20x	1.14E+09	3.1
	T8	10x	2.83E+08	1.5
	T8	20x	3.22E+08	0.9
3	T6	20x	4.65E+08	1.3
	T8	20x	1.61E+09	4.4
	T10	20x	6.65E+09	3.6
	T12	20x	3.38E+09	1.8

	T12	2.2x	3.18E+08	17.4
4.1	T10	20x	4.26E+09	11.6
4.2	T10	20x	8.34E+09	22.8
4.3	T10	20x	1.30E+09	3.6
4.1	T12	20x	1.49E+09	4.1
4.2	T12	20x	2.58E+09	7.1
4.3	T12	20x	1.78E+09	4.9
5.1	T6	20x	8.87E+08	2.4
5.2	T6	20x	7.51E+08	2.1
s	T6	20x	2.08E+09	5.7
5.1	T8	20x	5.93E+09	16.2
5.2	T8	20x	3.84E+09	10.5
5.3	T8	20x	5.50E+08	1.5
5.1	T10	20x	1.82E+09	5
5.2	T10	20x	5.18E+09	14.2
5.3	T10	20x	3.33E+09	9.1
5.1	T12	20x	6.51E+09	17.8
5.2	T12	20x	4.66E+09	12.7
5.3	T12	20x	1.21E+09	3.3

3.3 Cystic Fibrosis *P. aeruginosa* clinical isolate 2 (CF2)

OD_{600} measurements of CF2 were recorded at two-hour intervals over a 12-hour period across three independent collections **(Figure 13)**. The growth curves demonstrated a steady increase in bacterial density over time, with consistent trends observed across technical repeats.

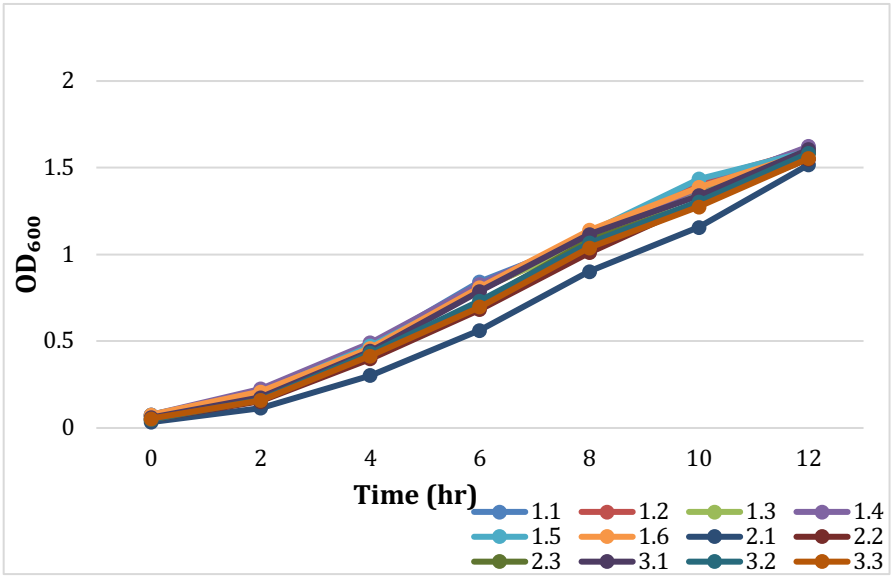

Figure 13. Growth curves of CF2.
OD_{600} measurements were recorded at 2-hour time intervals across 3 independent collections. Collection 1 included six technical repeats (Replicates 1.1–1.6), while Collections 2 and 3 included three technical repeats each. The x-axis represents time (hours), and the y-axis represents OD_{600}, serving as a proxy for bacterial cell density. The graph illustrates growth dynamics across collections.

Spot plating of CF2 was conducted at two-hour intervals to assess CFU counts, but due to the mucoid nature of the isolate, countable CFUs could not be obtained at any dilution **(Figure 14)**. Over time, serial dilutions ranging from 10^0 to 10^7 exhibited increased bacterial growth under light, confirming cell viability despite the inability to quantify individual colonies.

Next, NanoSight analysis was performed to quantify OMV concentrations from CF2 cultures at multiple timepoints **(Table 3)**. The highest OMV concentrations were detected at earlier timepoints. At T6, concentrations ranged from 1.45E+09 to 1.56E+10 particles/mL, while by T12, values had a greater range of 6.56E+07 to 3.91E+09 particles/mL.

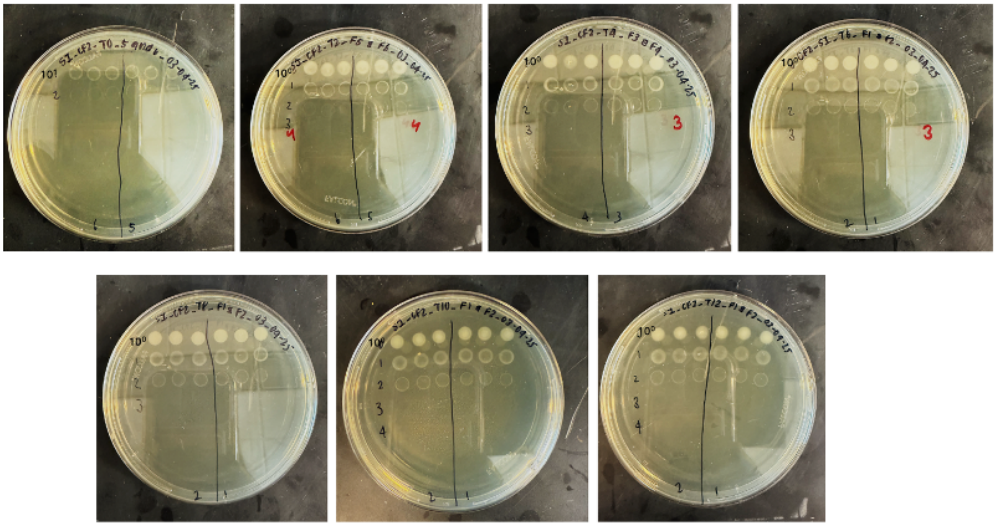

Figure 14. Spot Plating of CF2. Representative figure displays serial dilutions from 10^1 to 10^7, with three technical repeats for two different collections spotted on the same plate with three technical repeats per dilution across timepoints T0-T12. Due to the mucoid nature of the isolate, countable CFUs could not be obtained at any dilution.

Table 3. CF2 OMV counts from NanoSight.
This table presents NanoSight data for all isolated CF2 OMVs, including the average particle concentration (particles/mL) and particles per frame average at various timepoints with a 20x dilution factors.

CF2 NanoSight Counts				
Replicate	**Timepoint**	**Dilution factor**	**Concentration average (particles/mL)**	**Particles / frame average**
1.1	T6	20x	7.75E+09	21.2
1.2	T6	20x	4.11E+09	11.2
1.3	T6	20x	2.74E+09	7.5
1.4	T6	20x	1.56E+10	42.7
1.5	T6	20x	1.45E+09	4
1.6	T6	20x	5.45E+09	14.9
1.1	T8	20x	4.63E+09	12.6
1.2	T8	20x	3.04E+09	8.3
1.3	T8	20x	9.84E+09	26.9
1.4	T8	20x	5.73E+09	15.7
1.5	T8	20x	6.77E+09	18.5
1.6	T8	20x	9.58E+09	26.2
1.1	T10	20x	1.16E+09	63.3
1.2	T10	20x	1.05E+08	5.7
1.3	T10	20x	5.42E+07	3
1.4	T10	20x	1.83E+08	10
1.5	T10	20x	1.53E+08	8.4
1.6	T10	20x	1.44E+09	78.6
1.1	T10	20x	2.07E+09	5.6
1.2	T10	20x	4.08E+09	11.2
1.3	T10	20x	2.30E+09	6.3
1.4	T10	20x	3.34E+09	9.1
1.5	T10	20x	2.61E+09	7.1
1.6	T10	20x	1.16E+09	3.2
1.1	T12	20x	7.46E+07	4.1

1.2	T12	20x	2.05E+08	11.2
1.3	T12	20x	7.05E+07	3.9
1.4	T12	20x	1.32E+08	7.2
1.5	T12	20x	8.63E+07	4.7
1.6	T12	20x	6.56E+07	3.6
1.1	T12	20x	1.49E+09	4.1
1.2	T12	20x	3.91E+09	10.7
1.3	T12	20x	2.66E+09	7.3
1.4	T12	20x	2.23E+09	6.1
1.5	T12	20x	1.24E+09	3.4
1.6	T12	20x	2.19E+09	6

3.4 Comparative analysis between *P. aeruginosa* strains

Quantification of OMVs per cell across the three bacterial strains revealed distinct trends **(Figure 15)**. The number of OMVs per cell for each bacterial strain was calculated using NanoSight counts, determined by multiplying the concentration average (particles/mL) by the volume of OMVs. For samples with multiple concentration averages due to different dilution factors, the mean OMV count was used. PAO1 exhibited a general decrease in OMV counts over time. In contrast, CF1 and CF2 displayed more stable OMV levels, with CF2 showing highest overall OMV production at later timepoints.

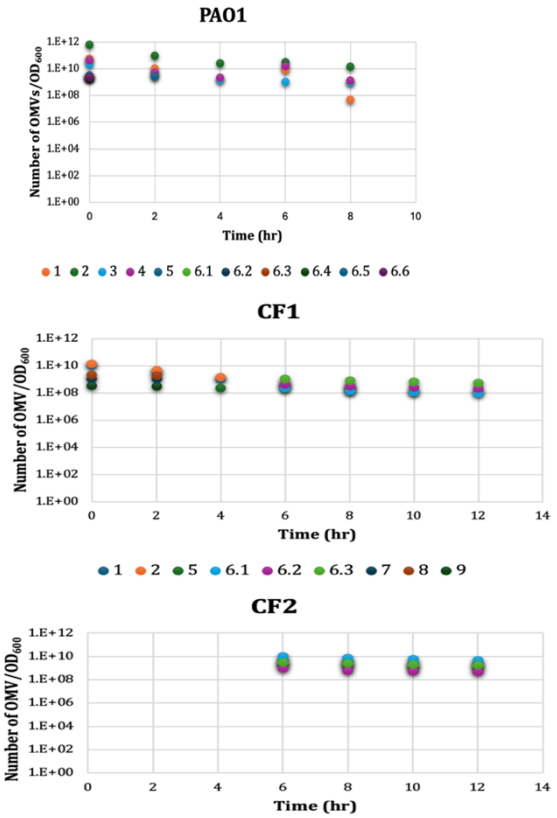

Figure 15. Number of OMVs per cell for each bacterial strain. OMV counts per cell are shown for PAO1 **(Top)**, CF1 **(Middle)**, and CF2 **(Bottom)**. OD_{600} served as a proxy for cell number. PAO1 exhibits a decline in OMVs per cell over time, while CF1 and CF2 maintain more stable levels. Note that graphs were sized to align timepoints vertically.

To assess NFAT and CREB activation across strains, OMVs from each timepoint were pooled for each strain and reconcentrated to 500 µL before incubation with THP-1 reporter cell lines and luminescence analysis. The total OMV count in each pooled sample was calculated by summing the counts from individual timepoints. For example, CF1 OMVs from T6, T8, T10, and T12 were combined, and the total OMV concentration was determined by aggregating their respective counts based on the volume concentrated and the averaged concentration from pooled

samples **(Table 4)**. This approach ensured that the assays reflected the cumulative OMV production of each strain rather than a single timepoint.

Table 4. Cumulative OMV counts obtained from NanoSight.
This table presents NanoSight data for all bacterial strains, including the average particle concentration (particles/mL) and particles per frame average at various timepoints using 20x and 50x dilution factors. OMVs from all timepoints were pooled for each bacterial strain.

Cumulative OMV Counts				
Bacterial strain	**Timepoint**	**Dilution factor**	**Concentration average (particles/mL)**	**Particles / frame average**
PAO1	T6	20x	9.55E+08	45
PAO1	T6	50x	1.33E+09	36.4
CF1	T6	20x	7.98E+08	38.3
CF1	T6	50x	9.48E+08	19.3
CF1	T8	20x	2.87E+08	9.2
CF1	T8	50x	3.68E+08	3
CF1	T10	20x	9.85E+08	25.8
CF1	T10	50x	6.62E+08	8.6
CF1	T12	20x	8.52E+08	20.6
CF1	T12	50x	5.82E+08	7.2
CF2	T6	20x	1.13E+09	51.3
CF2	T6	50x	5.82E+08	7.2
CF2	T8	20x	1.65E+09	356.1
CF2	T8	50x	7.85E+08	13.6
CF2	T10	20x	1.32E+09	68.2
CF2	T10	50x	5.09E+08	15.4
CF2	T12	20x	2.00E+09	104.8
CF2	T12	50x	5.05E+08	7.4

Bioluminescence assays measuring CREB activation (cAMP pathway) reveals strain-dependent responses **(Figure 16)**.

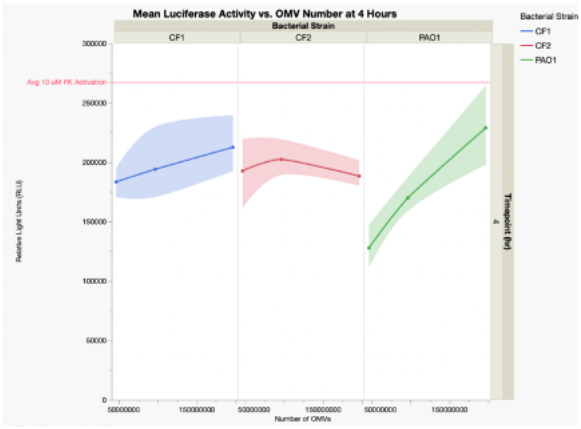

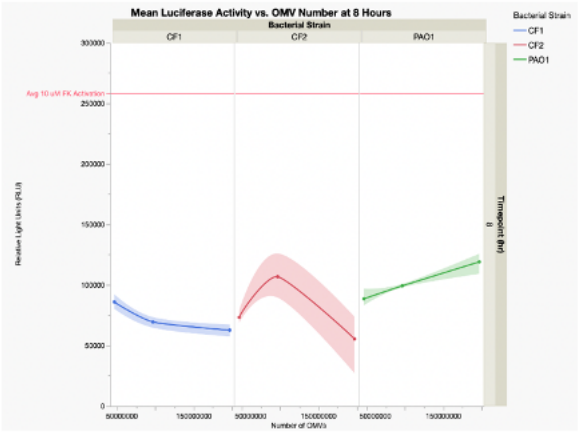

Figure 16. Activation profile of THP-1 CREB reporter line with OMVs from all three strains.
Luminescence was measured at 4-hour **(Top)** and 8-hour **(Bottom)** timepoints using OMVs (50, 100, 200 x 10^6) from each strain to assess CREB activation. Colored dots show mean RLU values, with lines indicating smoothed trends. Forskolin (10 µM) was used as a reference based on PAO1 assays.

At 4 hours, PAO1 exhibited a strong linear increase in CREB activation with increasing OMV concentrations (50, 100, and 200 x 10^6), indicating a dose-dependent effect. CF1 also followed a linear trend but with a less pronounced slope. In contrast, CF2 showed a peak response at 100 x 10^6 OMVs, followed by a decline, suggesting a potential activation threshold. By 8 hours, CREB activation decreased across all strains. CF1 displayed an inverse relationship with OMV number, while CF2 again peaked at 100 x 10^6 OMVs, this time with a sharper peak and steeper decline. PAO1 maintained a direct correlation, though with a shallower slope, indicating a more gradual activation response.

NFAT activation also varied significantly across strains and timepoints **(Figure 17).** At 4 hours, CF1 and CF2 exhibited opposite trends: CF1 peaked at 100 million OMVs, whereas CF2 showed a decreasing response, reaching its lowest activation at the same concentration. PAO1 displayed a moderate response, with the highest activation observed at 200 million OMVs. By 8 hours, CF1 and CF2 responses reversed—CF1 exhibited a declining trend, with the lowest activation at 100 million OMVs, while CF2 peaked at this amount. PAO1 maintained a consistent dose-dependent relationship, where increasing OMV concentrations corresponded to higher NFAT activation.

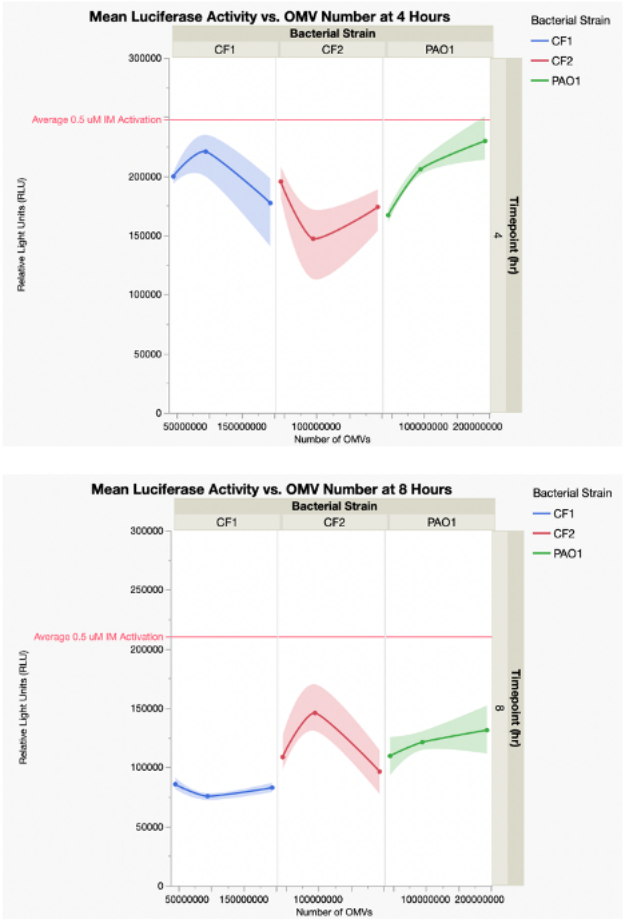

Figure 17. Activation profile of THP-1 NFAT reporter line with OMVs from all three strains. Luminescence was measured at 4-hour **(Top)** and 8-hour **(Bottom)** using OMVs (50, 100, 200 x 10^6) from each strain to assess NFAT activation. Colored dots show mean RLU values, with lines indicating smoothed trends. Ionomycin (0.5 µM) was used as a reference based on PAO1 assays.

Overall, these findings suggest that OMVs from the lab-adapted strain of *P. aeruginosa,* PAO1, consistently induce NFAT and CREB activation in THP-1 reporter cell lines. By contrast, OMVs from CF clinical isolates CF1 and CF2 exhibit more dynamic, time- and dose-dependent responses in THP-1 reporter cell lines.

4. Discussion

The results of our study demonstrate a generally consistent pattern for PAO1, where higher OMV concentrations correspond to increased activation of CREB and NFAT, indicative of greater cAMP and calcium signaling in recipient cells. This trend aligns with expectations, as elevated cAMP levels enhance activation in epithelial and immune cells. Therefore, a higher OMV load likely elicits a stronger activation response for monocytes, perhaps reflecting the perception of an increased extracellular bacterial burden and the corresponding need for enhanced host clearance mechanisms.

NanoSight quantification indicates that PAO1 generally produces more OMVs per cell than the clinical isolates and exhibits a decreasing trend in OMV production over time, whereas the clinical isolates maintain relatively stable OMV levels. One potential explanation is that, as a laboratory strain, PAO1 has not been conditioned to a physiological environment, unlike the clinical isolates, which have adapted to a host environment. Consequently, clinical isolates may be more efficient in packaging cargo into a smaller number of OMVs, allowing them to achieve similar functional effects with lower OMV output compared to PAO1. Additionally, it may indicate a more regulated response that minimizes bacterial clearance while fostering tolerance within the host environment. This suggests potential differences in OMV biogenesis between laboratory-adapted and clinically derived strains.

Compared to PAO1, the activation patterns induced in THP-1 reporter cell lines by OMVs from the two CF clinical isolates appear more variable. These differences between PAO1 and the clinical isolates underscore the complexity of host-pathogen interactions and suggest that strain-specific variations in OMV composition or host adaptation strategies may shape signaling dynamics over time. The relatively flat CREB response in CF2 at 4 hours suggests that its OMVs may be less effective at initiating early cAMP-mediated signaling. In contrast, the peak activation at 100 million OMVs by 8 hours implies a delayed yet coordinated signaling response. Similarly, the stabilization of CREB and NFAT responses in CF1 by 8 hours suggests that OMV-mediated activation of these pathways may reach a plateau, resulting in a more uniform signaling output. These findings highlight the potential for strain-specific OMV properties to influence the magnitude of host cell activation.

Across all strains, activation levels decrease at the 8-hour timepoint. This decline may reflect a resolution phase in cellular signaling, where sustained exposure to OMVs leads to

regulatory feedback mechanisms that dampen activation. Additionally, prolonged incubation may result in increased OMV degradation or uptake, reducing the effective concentration of OMVs available for stimulation.

These findings should be interpreted with the acknowledgment that some OMVs produced by the strains may not have been captured in the analysis. The NTA software used in this study is optimized for detecting particles within the 70–150 nm size range, meaning that OMVs smaller than 70 nm would not be detected. This limitation suggests that the total OMV population may be underestimated, potentially impacting the observed distribution and quantitative assessments.

Future directions include comprehensive analyses of the OMV proteome, secretome, and transcriptome to better characterize strain-specific differences. Incorporating monocytes derived from diverse human populations will also provide valuable insight into host-specific adaptations to bacterial presence.

5. Anthropological implications

Previous studies have shown that human populations have diverged in immune response-related genes due to distinct environmental exposures and selective pressures from pathogens. This divergence has led to population-specific polymorphisms that regulate stress responses. One well-documented example is the CCR5-Δ32 genetic polymorphism, which is most prevalent in northern Europe and western Asia (Novembre et al., 2005). Homozygous carriers of this mutation are resistant to HIV-1 infection because it inhibits functional expression of the CCR5 chemokine receptor, which is critical for cells to be infected by the virus (Ni et al., 2018). Smallpox has been proposed as a selective pressure maintaining this mutation, exemplifying how host-pathogen interactions shape immune system variation across populations. Other prominent examples include the potential selection of pyrin gene mutations, causing Familial Mediterranean Fever in homozygotes due to potential protection against the plague bacterium in carriers (Park et al., 2020).

While these prior studies have focused on how host traits may overcome virulence signals from pathogens, our study expands this framework by assessing non-lethal activation of cAMP and calcium signaling in monocytes by OMVs. OMVs consist of complex packages of secreted proteins, lipids, and nucleic acids and can signal virulence but also tolerance by modulating the host immune system in non-adversarial ways (Charpentier et al., 2023). By initiating the analysis of disparities in signaling dynamics of live monocytes exposed to lab-adapted vs. human-adapted isolates of the common pathogen *P. aeruginosa*, this research contributes to our understanding of population-specific immune adaptations, reinforcing existing knowledge while uncovering potential new mechanisms underlying host-pathogen adaptation and, in future studies, potential human subgroup divergence.

6. References

Augustyniak, D., Olszak, T., and Drulis-Kawa, Z. (2022). Outer Membrane Vesicles (OMVs) of Pseudomonas aeruginosa Provide Passive Resistance but Not Sensitization to LPS-Specific Phages. *Viruses* 14, 121. doi: 10.3390/v14010121

Bosshart, H., and Heinzelmann, M. (2016). THP-1 cells as a model for human monocytes. *Ann. Transl. Med.* 4, 438. doi: 10.21037/atm.2016.08.53

Bozoky, Z., Ahmadi, S., Milman, T., Kim, T. H., Du, K., Di Paola, M., et al. (2017). Synergy of cAMP and calcium signaling pathways in CFTR regulation. *Proc. Natl. Acad. Sci.* 114, E2086–E2095. doi: 10.1073/pnas.1613546114

Cantero, M. del R., Velázquez, I. F., Streets, A. J., Ong, A. C. M., and Cantiello, H. F. (2015). The cAMP Signaling Pathway and Direct Protein Kinase A Phosphorylation Regulate Polycystin-2 (TRPP2) Channel Function. *J. Biol. Chem.* 290, 23888. doi: 10.1074/jbc.M115.661082

Charpentier, L. A., Dolben, E. F., Hendricks, M. R., Hogan, D. A., Bomberger, J. M., and Stanton, B. A. (2023). Bacterial Outer Membrane Vesicles and Immune Modulation of the Host. *Membranes* 13, 752. doi: 10.3390/membranes13090752

Chen, Q., Shen, Y., and Zheng, J. (2021). A review of cystic fibrosis: Basic and clinical aspects. *Anim. Models Exp. Med.* 4, 220–232. doi: 10.1002/ame2.12180

Clapham, D. E. (2007). Calcium Signaling. *Cell* 131, 1047–1058. doi: 10.1016/j.cell.2007.11.028

De Lorenzo, G., Ferrari, S., Cervone, F., and Okun, E. (2018). Extracellular DAMPs in Plants and Mammals: Immunity, Tissue Damage and Repair. *Trends Immunol.* 39, 937–950. doi: 10.1016/j.it.2018.09.006

De Petrocellis, L., Starowicz, K., Moriello, A. S., Vivese, M., Orlando, P., and Di Marzo, V. (2007). Regulation of transient receptor potential channels of melastatin type 8 (TRPM8): Effect of cAMP, cannabinoid CB1 receptors and endovanilloids. *Exp. Cell Res.* 313, 1911–1920. doi: 10.1016/j.yexcr.2007.01.008

Endo, M. (2006). Calcium Ion as a Second Messenger With Special Reference to Excitation-Contraction Coupling. *J. Pharmacol. Sci.* 100, 519–524. doi: 10.1254/jphs.CPJ06004X

Ernst, O., Glucksam-Galnoy, Y., Athamna, M., Ben-Dror, I., Ben-Arosh, H., Levy-Rimler, G., et al. (2019). The cAMP Pathway Amplifies Early MyD88-Dependent and Type I Interferon-Independent LPS-Induced Interleukin-10 Expression in Mouse Macrophages. *Mediators Inflamm.* 2019, 3451461. doi: 10.1155/2019/3451461

Fuchs, E. L., Brutinel, E. D., Klem, E. R., Fehr, A. R., Yahr, T. L., and Wolfgang, M. C. (2010). In vitro and in vivo characterization of the Pseudomonas aeruginosa cyclic AMP (cAMP)

phosphodiesterase CpdA, required for cAMP homeostasis and virulence factor regulation. *J. Bacteriol.* 192, 2779–2790. doi: 10.1128/JB.00168-10

González-Espinosa, C., and Guzmán-Mejía, F. (2014). "8 - Basic Elements of Signal Transduction Pathways Involved in Chemical Neurotransmission," in *Identification of Neural Markers Accompanying Memory*, ed. A. Meneses (San Diego: Elsevier), 121–133. doi: 10.1016/B978-0-12-408139-0.00008-0

Grebert, C., Becq, F., and Vandebrouck, C. (2019). Focus on TRP channels in cystic fibrosis. *Cell Calcium* 81, 29–37. doi: 10.1016/j.ceca.2019.05.007

Guragain, M., King, M. M., Williamson, K. S., Pérez-Osorio, A. C., Akiyama, T., Khanam, S., et al. (2016). The Pseudomonas aeruginosa PAO1 Two-Component Regulator CarSR Regulates Calcium Homeostasis and Calcium-Induced Virulence Factor Production through Its Regulatory Targets CarO and CarP. *J. Bacteriol.* 198, 951–963. doi: 10.1128/jb.00963-15

Halls, M. L., and Cooper, D. M. (2011). Regulation by Ca2+-Signaling Pathways of Adenylyl Cyclases. *Cold Spring Harb. Perspect. Biol.* 3, a004143. doi: 10.1101/cshperspect.a004143

Hanssens, L. S., Duchateau, J., and Casimir, G. J. (2021). CFTR Protein: Not Just a Chloride Channel? *Cells* 10, 2844. doi: 10.3390/cells10112844

Hasan, R., and Zhang, X. (2018). Ca2+ Regulation of TRP Ion Channels. *Int. J. Mol. Sci.* 19, 1256. doi: 10.3390/ijms19041256

Hofer, A. M. (2012). Interactions between calcium and cAMP signaling. *Curr. Med. Chem.* 19, 5768–5773. doi: 10.2174/092986712804143286

Hofer, A. M., and Lefkimmiatis, K. (2007). Extracellular Calcium and cAMP: Second Messengers as "Third Messengers"? *Physiology* 22, 320–327. doi: 10.1152/physiol.00019.2007

King, M. M., Kayastha, B. B., Patrauchan, M. A., and Franklin, M. J. (2020). Calcium Regulation of Bacterial Virulence. *Adv. Exp. Med. Biol.* 1131, 827. doi: 10.1007/978-3-030-12457-1_33

Klockgether, J., Munder, A., Neugebauer, J., Davenport, C. F., Stanke, F., Larbig, K. D., et al. (2010). Genome Diversity of Pseudomonas aeruginosa PAO1 Laboratory Strains. *J. Bacteriol.* 192, 1113–1121. doi: 10.1128/JB.01515-09

Levring, J., Terry, D. S., Kilic, Z., Fitzgerald, G., Blanchard, S. C., and Chen, J. (2023). CFTR function, pathology and pharmacology at single-molecule resolution. *Nature* 616, 606–614. doi: 10.1038/s41586-023-05854-7

Malhotra, S., Hayes, D., and Wozniak, D. J. (2019). Cystic Fibrosis and Pseudomonas aeruginosa: the Host-Microbe Interface. *Clin. Microbiol. Rev.* 32, 10.1128/cmr.00138-18. doi: 10.1128/cmr.00138-18

McDonough, K. A., and Rodriguez, A. (2012). The myriad roles of cyclic AMP in microbial pathogens: from signal to sword. *Nat. Rev. Microbiol.* 10, 27–38. doi: 10.1038/nrmicro2688

Murabito, A., Bhatt, J., and Ghigo, A. (2023). It Takes Two to Tango! Protein–Protein Interactions behind cAMP-Mediated CFTR Regulation. *Int. J. Mol. Sci.* 24, 10538. doi: 10.3390/ijms241310538

Newton, A. C., Bootman, M. D., and Scott, J. D. (2016). Second Messengers. *Cold Spring Harb. Perspect. Biol.* 8, a005926. doi: 10.1101/cshperspect.a005926

Nguyen, J. P., Bianca, M., Huff, R. D., Tiessen, N., Inman, M. D., and Hirota, J. A. (2021). Modulation of cAMP metabolism for CFTR potentiation in human airway epithelial cells. *Sci. Rep.* 11, 904. doi: 10.1038/s41598-020-79555-w

Ni, J., Wang, D., and Wang, S. (2018). The CCR5-Delta32 Genetic Polymorphism and HIV-1 Infection Susceptibility: a Meta-analysis. *Open Med.* 13, 467. doi: 10.1515/med-2018-0062

Novembre, J., Galvani, A. P., and Slatkin, M. (2005). The Geographic Spread of the CCR5 Δ32 HIV-Resistance Allele. *PLOS Biol.* 3, e339. doi: 10.1371/journal.pbio.0030339

Park, Y. H., Remmers, E. F., Lee, W., Ombrello, A. K., Chung, L. K., Shilei, Z., et al. (2020). Ancient familial Mediterranean fever mutations in human pyrin and resistance to Yersinia pestis. *Nat. Immunol.* 21, 857–867. doi: 10.1038/s41590-020-0705-6

Patra, C., Foster, K., Corley, J. E., Dimri, M., and Brady, M. F. (2024). "Biochemistry, cAMP," in *StatPearls*, (Treasure Island (FL): StatPearls Publishing). Available at: http://www.ncbi.nlm.nih.gov/books/NBK535431/ (Accessed November 12, 2024).

Qin, S., Xiao, W., Zhou, C., Pu, Q., Deng, X., Lan, L., et al. (2022). Pseudomonas aeruginosa: pathogenesis, virulence factors, antibiotic resistance, interaction with host, technology advances and emerging therapeutics. *Signal Transduct. Target. Ther.* 7, 1–27. doi: 10.1038/s41392-022-01056-1

Rajasekaran, S., Maxvold, N. J., and Bunchman, T. E. (2011). "Chapter 71 - Glomerulotubular Dysfunction and Acute Kidney Injury," in *Pediatric Critical Care (Fourth Edition)*, eds. B. P. Fuhrman and J. J. Zimmerman (Saint Louis: Mosby), 1016–1035. doi: 10.1016/B978-0-323-07307-3.10071-0

Rosenberger, C. M., and Finlay, B. B. (2003). Phagocyte sabotage: disruption of macrophage signalling by bacterial pathogens. *Nat. Rev. Mol. Cell Biol.* 4, 385–396. doi: 10.1038/nrm1104

Sangiorgio, G., Nicitra, E., Bivona, D., Bonomo, C., Bonacci, P., Santagati, M., et al. (2024). Interactions of Gram-Positive Bacterial Membrane Vesicles and Hosts: Updates and Future Directions. *Int. J. Mol. Sci.* 25, 2904. doi: 10.3390/ijms25052904

Sarkisova, S. A., Lotlikar, S. R., Guragain, M., Kubat, R., Cloud, J., Franklin, M. J., et al. (2014). A Pseudomonas aeruginosa EF-Hand Protein, EfhP (PA4107), Modulates Stress Responses and Virulence at High Calcium Concentration. *PLoS ONE* 9, e98985. doi: 10.1371/journal.pone.0098985

Sartorio, M. G., Pardue, E. J., Feldman, M. F., and Haurat, M. F. (2021). Bacterial Outer Membrane Vesicles: From Discovery to Applications. *Annu. Rev. Microbiol.* 75, 609. doi: 10.1146/annurev-micro-052821-031444

Sassone-Corsi, P. (2012). The Cyclic AMP Pathway. *Cold Spring Harb. Perspect. Biol.* 4, a011148. doi: 10.1101/cshperspect.a011148

Saussereau, E., and Debarbieux, L. (2012). "Bacteriophages in the Experimental Treatment of *Pseudomonas aeruginosa* Infections in Mice," in *Advances in Virus Research*, eds. M. Łobocka and W. Szybalski (Academic Press), 123–141. doi: 10.1016/B978-0-12-394438-2.00004-9

Serezani, C. H., Ballinger, M. N., Aronoff, D. M., and Peters-Golden, M. (2008). Cyclic AMP. *Am. J. Respir. Cell Mol. Biol.* 39, 127–132. doi: 10.1165/rcmb.2008-0091TR

Tang, D., Kang, R., Coyne, C. B., Zeh, H. J., and Lotze, M. T. (2012). PAMPs and DAMPs: signal 0s that spur autophagy and immunity. *Immunol. Rev.* 249, 158. doi: 10.1111/j.1600-065X.2012.01146.x

THP-1 CRE-Luc2 - TIB-202-CRE-LUC2 | ATCC (n.d.). Available at: https://www.atcc.org/products/tib-202-cre-luc2 (Accessed November 12, 2024).

THP-1 NFAT-Luc2 - TIB-202-NFAT-LUC2 | ATCC (n.d.). Available at: https://www.atcc.org/products/tib-202-nfat-luc2 (Accessed November 12, 2024).

Tiku, V., and Tan, M.-W. (2021). Host immunity and cellular responses to bacterial outer membrane vesicles. *Trends Immunol.* 42, 1024–1036. doi: 10.1016/j.it.2021.09.006

Wang, H., Xu, J., Lazarovici, P., Quirion, R., and Zheng, W. (2018). cAMP Response Element-Binding Protein (CREB): A Possible Signaling Molecule Link in the Pathophysiology of Schizophrenia. *Front. Mol. Neurosci.* 11. doi: 10.3389/fnmol.2018.00255

Wu, W., Jin, Y., Bai, F., and Jin, S. (2015). "Chapter 41 - Pseudomonas aeruginosa," in *Molecular Medical Microbiology (Second Edition)*, eds. Y.-W. Tang, M. Sussman, D. Liu, I. Poxton, and J. Schwartzman (Boston: Academic Press), 753–767. doi: 10.1016/B978-0-12-397169-2.00041-X

Xie, Z., Wang, X., Huang, Y., Chen, S., Liu, M., Zhang, F., et al. (2024). *Pseudomonas aeruginosa* outer membrane vesicle-packed sRNAs can enter host cells and regulate

innate immune responses. *Microb. Pathog.* 188, 106562. doi: 10.1016/j.micpath.2024.106562

Zhang, M., Ma, Y., Ye, X., Zhang, N., Pan, L., and Wang, B. (2023). TRP (transient receptor potential) ion channel family: structures, biological functions and therapeutic interventions for diseases. *Signal Transduct. Target. Ther.* 8, 1–38. doi: 10.1038/s41392-023-01464-x

Zhang, P., Huang, C., Liu, H., Zhang, M., Liu, L., Zhai, Y., et al. (2024). The mechanism of the NFAT transcription factor family involved in oxidative stress response. *J. Cardiol.* 83, 30–36. doi: 10.1016/j.jjcc.2023.04.017

Zou, C., Zhang, Y., Liu, H., Wu, Y., and Zhou, X. (2022). Extracellular Vesicles: Recent Insights Into the Interaction Between Host and Pathogenic Bacteria. *Front. Immunol.* 13. doi: 10.3389/fimmu.2022.840550